A radial non-uniform helicon equilibrium discharge model*

Cheng Yu-Guo(成玉国), Cheng Mou-Sen(程谋森), Wang Mo-Ge(王墨戈)†, and Li Xiao-Kang(李小康)

College of Aerospace Science and Engineering, National University of Defense Technology, Changsha 410073, *China*

(Received 30 January 2014; revised manuscript received 28 March 2014; published online 20 August 2014)

Helicon discharges have attracted great attention in the electric propulsion community in recent years. To acquire the equilibrium properties, a self-consistent model is developed, which combines the helicon/ Trivelpiece–Gould (TG) waves-plasma interaction mechanism and the plasma flow theory under the confinement of the magnetic field. The calculations reproduce the central peak density phenomenon observed in the experiments. The results show that when operating in the wave coupling mode, high magnetic field strength B_0 results in the deviation of the central density versus B_0 from the linear relationship, while the density rise becomes flatter as the radiofrequency (rf) input power $P_{\rm rf}$ grows, and the electron temperature $T_{\rm e}$ radial profile is mainly determined by the characteristic of the rf energy deposition. The model could provide suggestions in choosing the B_0 and $P_{\rm rf}$ for medium power helicon thrusters.

Keywords: helicon discharges, magnetic field, radial properties, thruster

PACS: 52.75.Di, 52.50.Qt, 02.60.Cb, 88.85.J– **DOI:** 10.1088/1674-1056/23/10/105202

1. Introduction

While the helicon plasma source has been well known as the ion source in the variable specific impulse magneto-plasma rocket (VASIMR),[1,2] there is a growing interest in its usage as an electrodeless thruster, which avoids the electrode corruption problem that occurs in many thrusters.[3,4] Recently, several concepts have been presented, e.g. the helicon double layer thruster (HDLT),[5,6] other compact plasma thrusters,[7–10] etc. However, for the propulsion application, there is a limited understanding of the behavior of the equilibrium discharge properties in a thruster.

Early studies of the helicon ionization mechanisms were elaborated in Refs. [11] and [12], in which the Landau damping was recognized as a dominant mechanism for radiofrequency (rf) power deposition between the antenna and the plasma. The Trivelpiece–Gould (TG) modes were not discovered until the electron mass was taken into account in the fluid model, which was implemented to solve the possible wave branches.[13–17] Now, there is a consensus that the high ionization mechanism of the helicon discharges lies in the strong damping of the TG modes. Although numerous codes[18–20] based on this theory have been developed, studies of equilibrium discharge properties are relatively rare.

Numerical studies on the thermodynamic processes can be traced to Suwon,[21] in which a uniform global discharge model derived from Liebermann and Litchtenberg's work[22] was presented. In that model, the plasma density was assumed to be uniform in the bulk and decreased rapidly in the sheath region, and the magnetic field effect was indirectly manifested by the energy deposition process, and its influences on the plasma flow were not discussed. Thus, this is not suitable for the practical helicon discharges, which usually have non-uniform radial density profiles and are under the magnetic confinement.

Fruchtman *et al.*[23] developed a variable separation technique and studied the two-dimensional (2D) effects of the helicon discharges. Ahedo[24] presented a one-dimensional (1D) parametric analysis of the magnetized cylindrical plasmas, in which study it was found that the plasma response was fully characterized by the electron gyroradius, the electron and the ion collision mean free-free-paths. Then, this model was generalized to the 2D case[25] to study the plasma flow inside a discharge tube, which gave an insight into the helicon discharges. However, the rf power deposition process between the antenna and the plasma was neglected in these calculations. As a result, $T_{\rm e}$ was assumed to be uniform, and the electrons were assumed to be hot, which is not the case in the medium rf power discharges with $T_{\rm e}$ being between 2 eV–8 eV.

Recently, Curreli and Chen[26,27] proposed a self-consistent radial non-uniform helicon discharge model, in which the radial distributions of $T_{\rm e}$ and $n_{\rm e}$ were iteratively solved. In this model the magnetic confinement effects on the plasma fluid properties are neglected.

In this paper, we report the development of a non-uniform model describing the radial behaviors of the helicon discharges. This model mainly considers the helicon/TG waves-plasma interaction mechanism and the plasma flow theory under the confinement of the magnetic field. The rest of this paper is organized as follows. In Section 2 the developed basic plasma fluid model is depicted. In Section 3, the subsequent discussion on the thermodynamic properties of the helicon discharges in the uniform $T_{\rm e}$ case is given. In Section 4, the wave-

*Project supported by the National Natural Science Foundation of China (Grant No. 11305265).

†Corresponding author. E-mail: tlothf@126.com

© 2014 Chinese Physical Society and IOP Publishing Ltd

plasma interaction theory is first described briefly, and then the energy balance theory is presented. The comparisons between experimental results and simulation results are made in Section 5. The variations of fluid properties with non-uniform T_e are presented in Section 6. Finally, some conclusions are drawn from the present study in Section 7.

2. Basic theory and assumption

Assuming that the plasma is quasi-neutral, macroscopic conservations of mass, momentum for the electrons and ions are

$$\nabla \cdot n_e \boldsymbol{u}_e = n_e \nu_{iz}, \tag{1}$$

$$\nabla \cdot n_e \boldsymbol{u}_i = n_e \nu_{iz}, \tag{2}$$

$$m_e n_e \boldsymbol{u}_e \cdot \nabla \boldsymbol{u}_e = -\nabla n_e T_e - q n_e \nabla \phi + q n_e \boldsymbol{u}_e \times B_0 - m_e n_e (\nu_{en} + \nu_{iz}) \boldsymbol{u}_e, \tag{3}$$

$$m_i n_e \boldsymbol{u}_i \cdot \nabla \boldsymbol{u}_i = -\nabla n_e T_i - q n_e \nabla \phi + q n_e \boldsymbol{u}_i \times B_0 - m_i n_e (\nu_{in} + \nu_{iz}) \boldsymbol{u}_i. \tag{4}$$

Here, m_j and $\boldsymbol{u}_j$ are the mass and the velocity for species j ($j = $ e, i); q is the electric charge and the ions are assumed to be single ionization; ϕ is the electric potential; n_e is the plasma density; ν_{iz}, ν_{ei}, ν_{en}, and ν_{in} are the ionization, electron–ion, electron–neutral, and ion–neutral collision frequencies respectively.

For an axisymmetric problem, following a similar procedure to those of Hooper[28] and Ahedo and Merino,[29] the vectorial magnitudes are decomposed into the longitudinal (parallel to $\boldsymbol{B}_0$) and azimuthal components as follows:

$$\boldsymbol{u}_j = \tilde{\boldsymbol{u}}_j + u_{\theta j} \boldsymbol{l}_\theta, \tag{5}$$

where $\boldsymbol{l}_\theta$ is the azimuthal unit vector, $\tilde{\boldsymbol{u}}_j \cdot \boldsymbol{l}_\theta = 0$, and $u_{\theta j}$ is the azimuthal velocity. In the helicon plasma source tube, $\boldsymbol{B}_0$ generated by the solenoid or the Helmholtz coils is almost uniformly distributed along the axial direction.

Assuming macroscopic stationary and radial ambipolar diffusion, and neglecting the axial velocity, the governing equations of the radial and azimuthal components for the plasmas are

$$\frac{1}{r}\frac{\mathrm{d}}{\mathrm{d}r}(r n_e u_r) = n_e \nu_{iz}, \tag{6}$$

$$m_i u_r \frac{\mathrm{d}u_r}{\mathrm{d}r} = -\frac{T_i}{n_e}\frac{\mathrm{d}n_e}{\mathrm{d}r} - e\frac{\mathrm{d}\phi}{\mathrm{d}r} - eB_0 u_{\theta i} - m_i (\nu_{in} + \nu_{iz}) u_r + m_i \frac{u_{\theta i}^2}{r}, \tag{7}$$

$$m_i u_r \frac{\mathrm{d}u_{\theta i}}{\mathrm{d}r} = -eB_0 u_r - m_i (\nu_{in} + \nu_{ei} + \nu_{iz}) u_{\theta i} - m_i \frac{u_{\theta i} u_r}{r}, \tag{8}$$

$$m_e u_r \frac{\mathrm{d}u_r}{\mathrm{d}r} = -\frac{T_e}{n_e}\frac{\mathrm{d}n_e}{\mathrm{d}r} + e\frac{\mathrm{d}\phi}{\mathrm{d}r} - eB_0 u_{\theta e} - m_e (\nu_{en} + \nu_{iz}) u_r + m_e \frac{u_{\theta e}^2}{r}, \tag{9}$$

$$m_e u_r \frac{\mathrm{d}u_{\theta e}}{\mathrm{d}r} = eB_0 u_r - m_e (\nu_{en} + \nu_{ei} + \nu_{iz}) u_{\theta e} - m_e \frac{u_{\theta e} u_r}{r}. \tag{10}$$

For the low temperature plasma discharges, several simplifications can be made.

1) Since $T_i \ll T_e$, the ion thermal pressure is neglected;

2) Compared with the ion inertia term, the electron inertia term involving pure radial velocity is negligible;

3) As demonstrated by Hooper[28] and Ahedo and Merino,[29] the ratio between the ion and electron azimuthal velocities is proportional to m_e/m_i, thus the ion azimuthal cyclotron can be neglected for both the collision and collisionless cases.

Using the above assumptions and combining Eqs. (7) and (9) to eliminate the electric potential, the differential equations for n_e, u_r, and $u_{\theta e}$ can be expressed as[24]

$$\frac{\mathrm{d}u_r}{\mathrm{d}r} + u_r \frac{\mathrm{d}\ln n_e}{\mathrm{d}r} + \frac{u_r}{r} = \nu_{iz}, \tag{11}$$

$$u_r \frac{\mathrm{d}u_{\theta e}}{\mathrm{d}r} + \frac{u_{\theta e} u_r}{r} = \frac{eB_0}{m_e} u_r - \nu_e u_{\theta e}, \tag{12}$$

$$u_r \frac{\mathrm{d}u_r}{\mathrm{d}r} + c_s^2 \frac{\mathrm{d}\ln n_e}{\mathrm{d}r} = \frac{m_e}{m_i}\frac{u_{\theta e}^2}{r} - \frac{eB_0}{m_i} u_{\theta e} - \nu_i u_r, \tag{13}$$

where $\nu_e = \nu_{iz} + \nu_{ei} + \nu_{en}$, $\nu_i = \nu_{in} + \nu_{iz}$,[24,26] and c_s is the Bohm velocity. For the axisymmetric configuration, the boundary condition at $r = 0$ is

$$u_r = u_{\theta e} = \ln \frac{n_e}{n_0} = 0, \tag{14}$$

where n_0 is the density in the center. In order to avoid singularity, here, we take the first order Taylor approximation of the radial functions at a location $r_0 \ll r_p$ (r_p is the plasma radius):

$$u_r|_{r_0} = \left.\frac{\mathrm{d}u_r}{\mathrm{d}r}\right|_{r=0} \cdot r_0 = \frac{\nu_{iz}}{2} r_0, \tag{15}$$

$$u_{\theta e}\Big|_{r_0} = \left.\frac{\mathrm{d}u_{\theta e}}{\mathrm{d}r}\right|_{r=0} \cdot r_0 = \frac{eB_0}{2m_e}\frac{\nu_{iz}}{\nu_{iz} + \nu_e} r_0, \tag{16}$$

$$\ln \frac{n_e}{n_0}\Big|_{r=0} = \left.\frac{\mathrm{d}\ln n_e}{\mathrm{d}r}\right|_{r=0} \cdot r_0 = \frac{1}{c_s^2}\left[-\left(\frac{\mathrm{d}u_r}{\mathrm{d}r}\right)^2 - \nu_i \frac{\mathrm{d}u_r}{\mathrm{d}r} - \frac{eB_0}{m_i}\frac{\mathrm{d}u_{\theta e}}{\mathrm{d}r} + \frac{m_e}{m_i}\left(\frac{\mathrm{d}u_{\theta e}}{\mathrm{d}r}\right)^2\right]\Bigg|_{r=0} r_0^2. \tag{17}$$

Equations (11)–(13) are then simultaneously solved using the fourth-order Runge–Kutta scheme, at rf $f = 13.56$ MHz, neutral pressure $p_0 = 3$ mTorr (1 Torr = 1.33322×10^2 Pa), and $r_p = 4$ cm.

3. Fluid properties under uniform T_e

Equations (11)–(13) can be integrated to give the radial profiles of n_e, u_r, and $u_{\theta e}$ under given p_0 when T_e is uniform. For most of low temperature plasma discharges, the sheath radial dimension is far less than the plasma radius, and the sheath effects on the macroscopic fluid properties can be neglected, thus, we assume that the ions reach Bohm velocity at the plasma edge.

In the typical helicon discharges, the values of n_e are between 10^{11} cm^{-3}–10^{13} cm^{-3}. Figure 1 shows the variations of T_e with B_0 in the central density range mentioned above. For any specified density level n_0, T_e descends monotonically as B_0 increases. The results show that T_e does not vary significantly for different values of n_0, and any particular density in this range, e.g. 10^{12} cm^{-3}, will be sufficient to make reliable predictions. Furthermore, since n_0 varies only with P_{rf} under the conditions given above, it can be reasonably deduced that the variation of P_{rf} has little influence on T_e. This is due to the fact that the ionization collisions consume the majority of the input energy for the medium power helicon discharge, thus the energy fraction for the temperature rise is small.

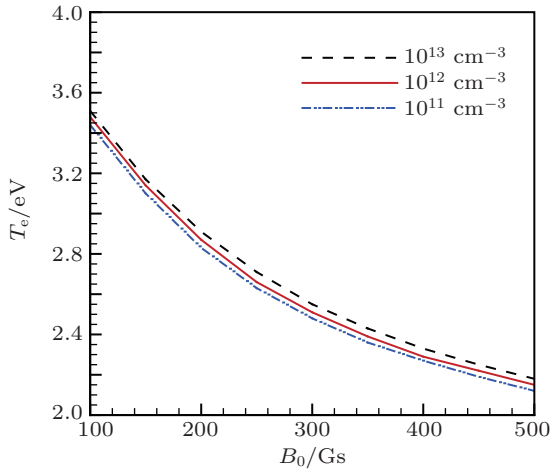


Fig. 1. (color online) Plots of electron temperature T_e versus B_0 for central plasma density $n_0 = 10^{11}$, 10^{12}, and 10^{13} cm^{-3}. The unit 1 Gs = 10^{-4} T.

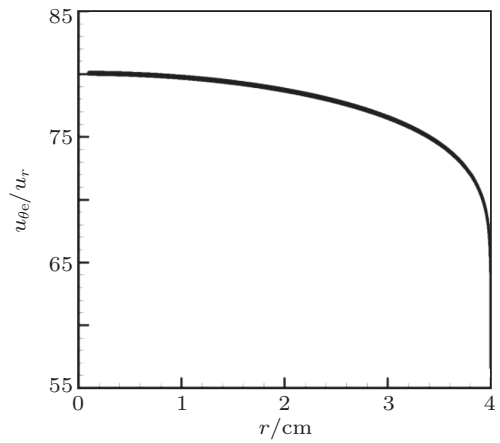


Fig. 2. (color online) The ratio of azimuthal $u_{\theta e}$ to radial u_r versus r at $B_0 = 500$ Gs.

In the bulk plasma as shown in Fig. 2, the ratio of $u_{\theta e}$ to u_r varies with r gradually. To explain this, we note that the following relationship:

$$\frac{u_r}{c_s} \ll 1 \tag{18}$$

holds in the bulk, which can be deduced from the combination of Fig. 3 with Fig. 4, and then equation (19) is obtained as

$$\frac{u_r}{c_s} \doteq 10^{-2}. \tag{19}$$

Equation (11)–(13) can be expressed as

$$\frac{\mathrm{d}u_r}{\mathrm{d}r} = \frac{eB_0}{m_i}\frac{u_{\theta e}u_r}{c_s^2} + \nu_i\frac{u_r^2}{c_s^2} + \nu_{iz} - \frac{u_r}{r}\frac{\frac{m_e}{m_i}u_{\theta e}^2 + c_s^2}{c_s^2}, \tag{20}$$

$$\frac{\mathrm{d}u_{\theta e}}{\mathrm{d}r} = \frac{eB_0}{m_e} - \nu_e\frac{u_{\theta e}}{u_r} - \frac{u_{\theta e}}{r}. \tag{21}$$

Meanwhile, the following approximations are satisfied:

$$\frac{eB_0}{m_i}\frac{u_{\theta e}u_r}{c_s^2} \sim 10^2,\ \nu_i\frac{u_r^2}{c_s^2} \sim 10^2,\ \nu_{iz} \sim 10^5,\ \frac{u_r}{r} \sim 10^3, \tag{22}$$

$$\frac{eB_0}{m_e} \sim 10^9,\ \nu_e\frac{u_{\theta e}}{u_r} \sim 10^6,\ \frac{u_{\theta e}}{r} \sim 10^3. \tag{23}$$

Then, equations (20) and (21) can be simplified into

$$\frac{\mathrm{d}u_r}{\mathrm{d}r} \sim \nu_{iz}, \tag{24}$$

$$\frac{\mathrm{d}u_{\theta e}}{\mathrm{d}r} \sim \frac{eB_0}{m_e}. \tag{25}$$

Equations (24) and (25) indicate approximately linear increase of the two velocities in the radial direction under the conditions of Eqs. (18) and (19), which results in the trend shown in Fig. 2.

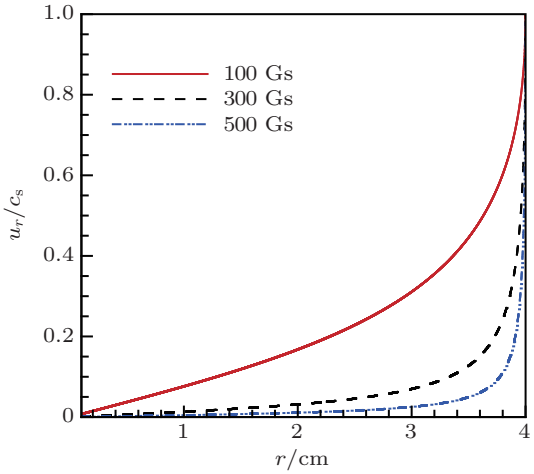


Fig. 3. (color online) Plots of ratio of azimuthal velocity u_r to c_s versus r for different values of B_0.

To examine the effect of neglecting B_0, the plasma radii are taken to be the same values in our calculation in accordance with Ref. [26]. The results are displayed in Fig. 5, showing that higher T_e is obtained when B_0 is neglected. As in the case of 0.3 mTorr, values of T_e are greater than 13 eV for $r_p = 2.5$ cm, and 25 eV for $r_p = 1.5$ cm, respectively.

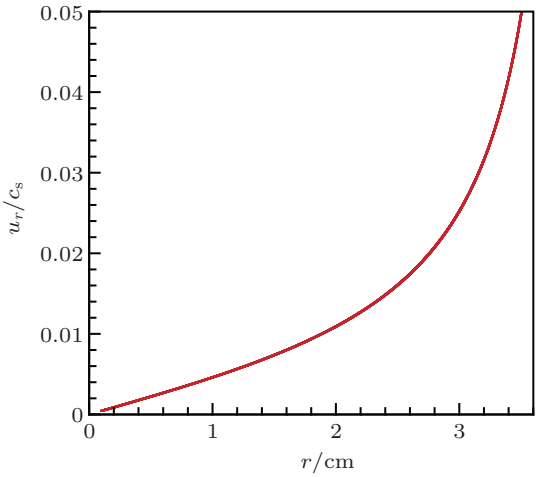


Fig. 4. (color online) Ratio of azimuthal velocity u_r to c_s versus r in the bulk at $B_0 = 500$ Gs.

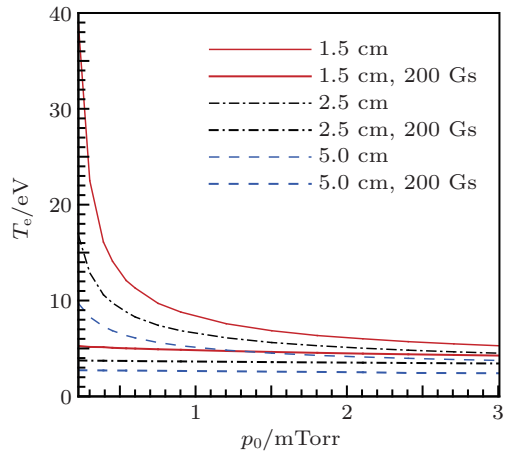


Fig. 5. (color online) Variations of electron temperature T_e with p_0 for different values of plasma radius r_p.

In fact, values of T_e measured in the medium power helicon discharge experiments[5,30] are usually between 2.0 eV–8.0 eV for the medium rf power. According to Curreli and Chen's[26] explanation, the inelastic threshold of argon is around 12 eV and the radiation loss will limit T_e to below 5 eV or so. Here, we have shown that the appropriate T_e can be obtained just by considering the finite B_0 effect (Fig. 5). Under the magnetic confinement, the azimuthal cyclotron consumes the energy absorbed (Fig. 2), which is a considerable energy loss channel.

4. Energy balance

Here, we follow a similar procedure to that in Ref. [19] to calculate the energy deposition under the antenna current $I_0 = 1$ A:

$$\mathrm{R_p} = \int_v P_v \mathrm{d}v = \int_v \mathrm{Re}\,(J \cdot E)\,\mathrm{d}v. \tag{26}$$

The deposited power into plasma P_{abs} with rf input power P_{rf} is

$$P_{abs} = \frac{2P_{rf}}{R_p + R_c} \int_0^{L_s} P_V \,\mathrm{d}z, \tag{27}$$

where R_c is the resistance of external transmission cables.

The energy loss at r is mainly due to the particle collisions and axial sheath. The former includes the neutral ionization, excitation, and elastic collisions, and the latter is caused by the plasma recombination at the tube ends.

The ionization cost per particle is

$$\varepsilon_c = \frac{(K_{iz}\varepsilon_{iz} + K_{ex}\varepsilon_{ex} + K_{el}\varepsilon_{el})}{K_{iz}}, \tag{28}$$

where ε_{iz}, ε_{ex}, and ε_{en} are the ionization, excitation, and elastic collision energies respectively, and K_{iz}, K_{ex}, and K_{en} are the corresponding rate constants.[24,26] The collisional energy loss then can be expressed as

$$P_{col} = L_s n_e \varepsilon_c \nu_{iz}. \tag{29}$$

As the axial sheath loss, the ion hits the wall with an energy of $V_s + 0.5T_e$, where V_s is the sheath voltage (for Ar^+, $V_s \approx 4.7T_e$), and the electron hits the wall with an energy of $2T_e$, thus each electron–ion recombination pair causes an energy loss of $\varepsilon_{sh} = V_s + 2.5T_e$. Then the wall sheath loss is

$$P_{sh} = 2n_e c_s \varepsilon_{sh}. \tag{30}$$

The energy balance equation should be expressed as

$$L_s \nabla \cdot \left(\frac{1}{2} m_e n_e \boldsymbol{u}_e^2 + \frac{p_e}{\gamma - 1} + p_e\right) \boldsymbol{u}_e = P_{abs} - P_{sh} - P_{col} - L_s e n_e \boldsymbol{u}_e \cdot \nabla\phi, \tag{31}$$

where p_e and γ are the electron pressure and specific heats ratio, respectively.

Equations (11)–(13) give the radial profiles of $n_e(r)$, which are used to calculate the $P_{abs}(r)$ via the wave–plasma interaction code, and the updated $T_e(r)$ solved by Eq. (31) is again taken into Eqs. (11)–(13). The procedure is repeated till the $n_e(r)$ and $T_e(r)$ are converged to the equilibrium values. In this model, we neglect the neutral depletion effect which means that the gas pressure is kept constant. According to some reported experiments on the helicon source thrusters, the actual ionization fraction is low and the neutral depletion effect will not change the plasma property significantly. So the model will not be applicable for the discharge conditions when the input power is tens to hundreds of kilowatts, in which the electrons are hot and the neutral gas is nearly completely ionized. In Section 3, the calculated results are in accordance with those from the global model in Ref. [22], which shows the reasonability of the model.

5. Comparison with the experiments

To verify the model, we take several experiments for example, which include the different exciting frequencies and the widely used antenna types.

Case 1 The experiment conducted by Toki *et al.*,[31] which has the following parameters: $r_p = 1.25$ cm, $B_0 = 45$ Gs, $p_0 = 50$ mTorr, argon, $f = 67.8$ MHz, $R_c = 0.2$ Ω, and the antenna is the double loop type.

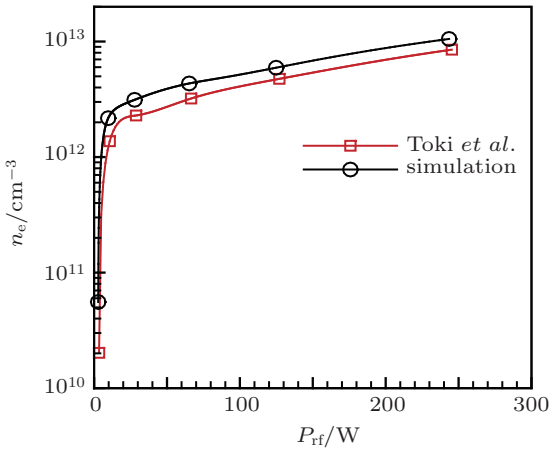


Fig. 6. (color online) Comparison of Toki *et al.*'s experiments with the simulation (central).

Case 2 The experiment conducted by Chen,[32] which has the following parameters: $r_p = 2.5$ cm, $B_0 = 80$ Gs, $p_0 = 20$ mTorr, argon, $f = 13.56$ MHz, $R_c = 0.6$ Ω, and the antenna is a type of single loop antenna.

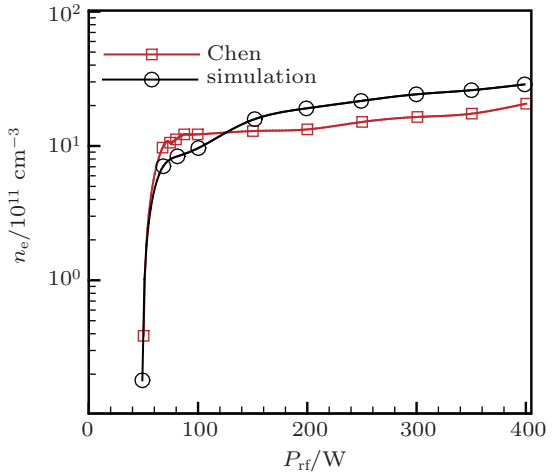


Fig. 7. (color online) Comparison of Chen's experimental results with the simulation results (radial averaged).

Figures 6 and 7 show the comparisons between the experimental results and the simulation results. It is obvious that the model developed can give appropriate approximations, which indicates that the model is capable of predicting the radial variation trend of the helicon discharge. The next section will give the detailed simulations of the radial discharge characteristics when B_0 and P_{rf} are varied.

6. Variations of fluid properties with non-uniform T_e

The exciting antenna with a radius of 4.2 cm and a length of 20 cm is used in the following calculations, which is a type of the $m = 1$ half-helical antenna, $R_c = 0.5$ Ω.

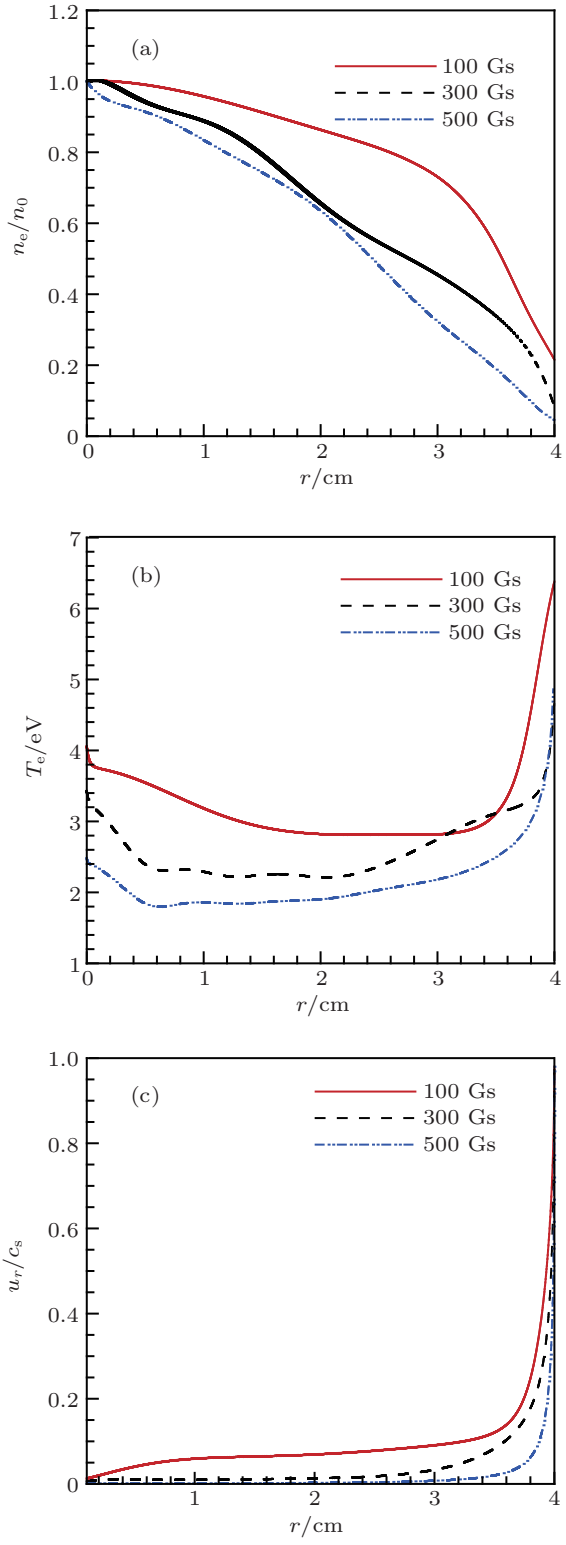


Fig. 8. (color online) (a) The ratio of radial plasma density n_e to central density n_0, (b) electron temperature T_e, and (c) the ratio of azimuthal velocity u_r to c_s versus r for different values of B_0.

Figure 8 shows the radial variations of the plasma thermodynamic parameters for B_0 of 100 Gs, 300 Gs, and 500 Gs. The central density peak characteristic is retained, although the main rf power absorption happens at the plasma edge. T_e shows large variation with B_0 and the radial variation trend is in accordance with the energy deposition profile. u_r remains low in the bulk and rises rapidly in the pre-sheath region.

Figure 8(b) shows that the central heating is significant, which is caused by the radial non-uniform density and is different from the uniform density case.

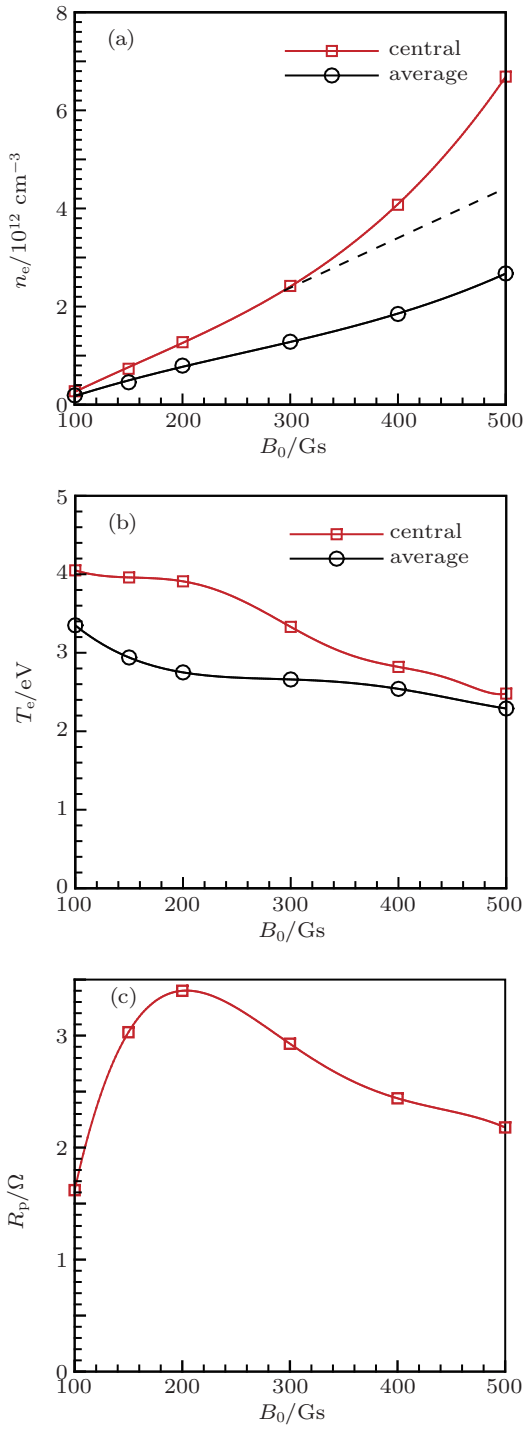


Fig. 9. (color online) Variations of (a) plasma density n_e, (b) electron temperature T_e, and (c) plasma resistance R_p with B_0 for the case $P_{rf} = 500$ W.

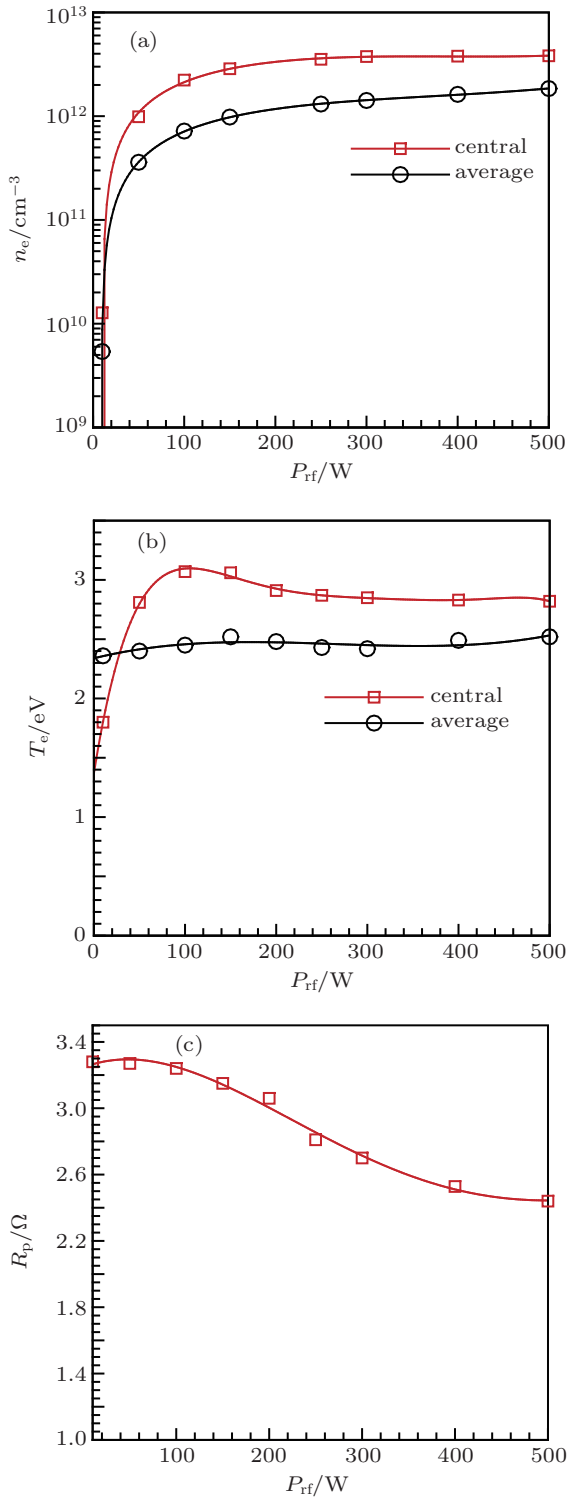


Fig. 10. (color online) Variations of (a) plasma density n_e, (b) electron temperature T_e, and (c) plasma resistance R_p versus P_{rf} for $B_0 = 400$ Gs.

Figure 9(a) shows the variations of the central and radial average values of n_e and T_e with B_0 at $P_{rf} = 500$ W. The average density versus B_0 follows linear relationship at low field strength, which has been observed in the experiments, and is in accordance with the wave dispersion relationship of the helicon waves. However, the central density slope changes when $B_0 > 300$ Gs. This could be explained as the fact that at higher B_0, the TG waves damp more quickly and the bulk plasma is

mainly heated by the helicon waves, which results in the more steepened profiles.

As shown in Fig. 9(b), T_e decreases as B_0 increases. At a constant input power, on the one hand, from Fig. 9(c), we can find that larger B_0 results in inefficient coupling between the antenna and the plasma; on the other hand, the growth of the plasma density consumes more energy, thus T_e decreases.

Figure 10 shows the variations of central and average n_e and T_e with rf input power at $B_0 = 400$ Gs. This figure shows that the plasma density increases rapidly from 10^{10} cm^{-3} at 10 W to about 10^{12} cm^{-3} at about 50 W rf input power, then the 'saturation' trend is evident. At low power, the main absorption is in the capacitively coupled mode, then, as P_{rf} increases, the discharge shifts to helicon/TG waves coupling region, when the sudden rise of the plasma density occurs.

Figure 10(a) shows that the increased P_{rf} leads to the flattened density profiles, which is different from the scenario in Fig. 10(a), and that the density is 'saturated' as P_{rf} grows. Since the corresponding central and average T_e in Fig. 10(b) remain stable, the increased energy is lost by the inefficient coupling between the antenna and the plasma as shown in Fig. 10(c).

7. Conclusions

A radial non-uniform helicon discharge model is studied. This model focuses on the radial plasma properties and can give reasonable predictions of the density, electron temperature varying with the magnetic field strength, and the rf input power. This model is applicable when the ionization fraction is low, so that the neutral depletion effects can be neglected. Using the model, we find that the T_e radial distribution is mainly determined by the energy deposition, and the density profiles show the central peak characteristics under different input parameters, which is consistent with the experimental results reported.

As B_0 increases, caused by the magnetic confinement and the TG wave edge damping, the density profile $n_e(r)$ becomes sharper. At higher B_0 (e.g. the electric propulsion application), the bulk radial velocity is low, which lessens the subsequent divergence of the plasma plume and enhances the energy conversion efficiency. However, the radial density is highly non-uniform in this case, which may lead to non-uniform thrust in turn.

As P_{rf} increases, the density will be 'saturated' due to the inefficient coupling, which limits the maximum thrust density and lessens the efficiency. However, at higher P_{rf}, the relatively flattened radial density and stable T_e are useful because they can enhance the working stability of the thruster.

References

[1] Longmier B W, Cassady L D, Ballenger M G, Carter M D, Chang-Diaz F R, Glover T W, Ilin A V, McCaskill G E, Olsen C S and Jared P Squire 2011 *J. Prop. Power* **27** 915

[2] Sheth R B, Ungar E K and Chambliss J P 2012 42*nd International Conference on Environmental Systems*, July 15–19, San Diego, USA, *AIAA* 2012-3497

[3] Cheng K and Pan W X 2009 *Chin. Phys. Lett.* **26** 1252013

[4] Zhang R, Zhang D X, Zhang F, He Z and Wu J J 2013 *Acta Phys. Sin.* **62** 025207 (in Chinese)

[5] West M D, Charles C and Boswell R W 2009 *J. Phys. D: Appl. Phys.* **42** 245021

[6] Takahashi K, Lafleur T, Charles C, Alexander P, Boswell R W, Perren M, Laine R, Pottinger S, Lappas V, Harle T and Lamprou D 2011 *Appl. Phys. Lett.* **98** 141503

[7] Batishchev O V 44th AIAA/ASME/SAE/ASEE 2008 *Joint Propulsion Conference & Exhibit*, July 21–23, Harford CT, USA, *AIAA* 2008-5293

[8] Beal B E and FabianM 2007 *International Electric Propulsion Conference*, September 17–20, Florence, Italy, 2007-162

[9] Palmer D D, Walker M L R, Manete M, Johan C, Cristina B and Daniele P 2008 44th AIAA/ASME/SAE/ASEE *Joint Propulsion Conference & Exhibit*, July 21–23, Harford CT, USA, *AIAA* 2008–4925

[10] Chen F F 2008 *IEEE Trans. Plasma Sci.* **36** 2095

[11] Boswell R W and Chen F F 1997 *IEEE Trans. Plasma Sci.* **25** 1229

[12] Chen F F and Boswell R W 1997 *IEEE Trans. Plasma Sci.* **25** 1245

[13] Shamrai K P and Taranov V B 1994 *Plasma Phys. Control Fusion* **36** 1719

[14] Shamrai K P and Taranov V B 1995 *Phys. Lett. A* **204** 139

[15] Shamrai K P and Taranov V B 1996 *Plasma Sources Sci. Technol.* **5** 474

[16] Shamrai K P, Pavlenko V P and Taranov V B 1997 *Plasma Phys. Control Fusion* **39** 505

[17] Blackwell D D, madziwa T G, Arnush D and Chen F F 2002 *Phys. Rev. Lett.* **88** 145002

[18] Suwon Cho 1996 *Phys. Plasmas* **3** 4268

[19] Arnush D and Chen F F 1998 *Phys. Plasmas* **5** 1239

[20] Shamrai K P and Shinohara S 2001 *Phys. Plasmas* **8** 4659

[21] Suwon Cho 1999 *Phys. Plasmas* **6** 359

[22] Lieberman M A and Litchtenberg A J 2005 *Principles of Plasma Discharges and Materials Processing*, 2nd edn. (New York: Wiley-Interscience), translated in Chinese by Pi Y K, *et al*. (in Chinese)

[23] Fruchtman A, Makrinich G and Ashkenazy J 2005 *Plasma Sources Sci. Technol.* **14** 152

[24] Ahedo E 2009 *Phys. Plasmas* **16** 113503

[25] Ahedo E and Jaume Navalarro-cavalle 2013 *Phys. Plasmas* **20** 043512

[26] Curreli D and Chen F F 2011 *Phys. Plasmas* **18** 113501

[27] Chen F F and Curreli D 2013 *Phys. Plasmas* **20** 057102

[28] Hooper E B 1993 *J. Prop. Power* **9** 757

[29] Ahedo E and Merino M 2010 *Phys. Plasmas* **17** 073501

[30] Gilland J, Breun R and Hershkowitz N 1998 *Plasma Source Sci. Technol.* **7** 416

[31] Toki K, Shinohara S, Tanikawa T and Shamrai K P 2006 *Thin Solid Films* **506–507** 597

[32] Chen F F 2007 *Plasma Sources Sci. Technol.* **16** 593